Hindawi Publishing Corporation
Shock and Vibration
Volume 2016, Article ID 1928086, 14 pages
http://dx.doi.org/10.1155/2016/1928086

Research Article

Vortex-Induced Vibration of a Cable-Stayed Bridge

M. T. Song,[1] D. Q. Cao,[2] and W. D. Zhu[2,3]

[1]*Faculty of Civil Engineering and Mechanics, Jiangsu University, Zhenjiang, Jiangsu 212013, China*
[2]*School of Astronautics, Harbin Institute of Technology, P.O. Box 137, Harbin 150001, China*
[3]*Department of Mechanical Engineering, University of Maryland, Baltimore County, Baltimore, MD 21250, USA*

Correspondence should be addressed to M. T. Song; songmt2004@163.com

Received 21 June 2015; Revised 13 October 2015; Accepted 15 October 2015

Academic Editor: Tai Thai

The dynamic response of a cable-stayed bridge that consists of a simply supported four-cable-stayed deck beam and two rigid towers, subjected to a distributed vortex shedding force on the deck beam with a uniform rectangular cross section, is studied in this work. The cable-stayed bridge is modeled as a continuous system, and the distributed vortex shedding force on the deck beam is modeled using Ehsan-Scanlan's model. Orthogonality conditions of exact mode shapes of the linearized undamped cable-stayed bridge model are employed to convert coupled governing partial differential equations of the original cable-stayed bridge model with damping to a set of ordinary differential equations by using Galerkin method. The dynamic response of the cable-stayed bridge is calculated using Runge-Kutta-Felhberg method in MATLAB for two cases with and without geometric nonlinear terms. Convergence of the dynamic response from Galerkin method is investigated. Numerical results show that the geometric nonlinearities of stay cables have significant influence on vortex-induced vibration of the cable-stayed bridge. There are different limit cycles in the case of neglecting the geometric nonlinear terms, and there are only one limit cycle and chaotic responses in the case of considering the geometric nonlinear terms.

1. Introduction

Vortex-induced vibration (VIV) of a long-span structure is of practical importance to bridge engineering after collapse of the Tacoma Narrows bridge in 1940 [1]. VIV of a structure immersed in a fluid flow results from forces generated by alternating shedding of vortices from its surface. The structural vibration interacts with the flow, changing the fluid forces acting on the structure, and strongly nonlinear structural response with multifrequencies takes place [2]. VIV may lead to failure of a cable-stayed bridge due to fatigue damage and affect travel safety and/or comfort levels of its occupants [3]. Hence, an accurate prediction of the response of the cable-stayed bridge to vortex shedding at an early design stage is essential.

To achieve this objective, computational fluid dynamics (CFD) techniques are widely adopted to compute fluid forces on the structure by calculating the flow field information. Major CFD approaches, including direct numerical simulation [4–7], the time-marching scheme [8], and the vortex-in-cell method [9–12], mostly directly or approximately solve the time-dependent Navier-Stokes equation; however, they are limited by heavy computational requirement, which is difficult to satisfy up to now.

Apart from numerical simulations, semiempirical models have emerged as an alternative approach for predicting VIV due to their simple forms. A detailed review on VIV modeling has been given by Gabbai and Benaroya [13], according to which semiempirical models can be divided into two main classes: single-degree-of-freedom (SDOF) models and wake-oscillator models. The former can be classified into negative-damping models [14–17] and force-coefficient data models [18–20]. The wake-oscillator models consider two variables: a structural response variable and a fluid dynamic variable (e.g., the lifting force) [21–26].

The above semiempirical models are not able to predict the structural response for any cross section shape of a bluff body since their model parameters rely on values of structural mass and damping. An empirical model of VIV of line-like structures with complex cross sections such as bridge decks, which requires few and relatively simple wind-tunnel tests, may be useful in practical applications. Ehsan and

Scanlan [27] proposed a SDOF model referred to as Ehsan-Scanlan's model, which satisfies the above requirement; a single wind-tunnel test with a relatively simple experimental setup, called the decay-to-resonance test, is needed to estimate its model parameters. Moreover, aeroelastic parameters identified on a section model can be used to calculate the response of a cable-stayed bridge considering actual model properties of the structure. Marra et al. [28] applied Ehsan-Scanlan's model in a realistic case study and proposed an alternative identification procedure based on direct numerical solution of a nonlinear ordinary differential equation.

Most previous studies mainly focus on VIV of cylindrical bodies and a deck-shaped body to study VIV of stay cables and a deck beam, respectively, which are two main components of a cable-stayed bridge. However, there is interaction between the stay cables and deck beam when they vibrate [29]. This paper presents VIV of a cable-stayed bridge that consists of a simply supported four-cable-stayed deck beam and two rigid towers, and it aims to study effects of the geometric nonlinearities of stay cables on the deck beam with a uniform rectangular cross section that is subjected to a vortex shedding force. Nonlinear and linear partial differential equations that govern transverse and longitudinal vibrations of the stay cables and transverse vibrations of segments of the deck beam, respectively, were derived along with their boundary and matching conditions using a Newtonian approach. Ehsan-Scanlan's model is used to model the vortex shedding force that is considered as a distributed force. Exact natural frequencies and mode shapes of the linearized undamped cable-stayed bridge model obtained in [29] are used to spatially discretize coupled governing partial differential equations of the original nonlinear cable-stayed bridge model with damping via Galerkin method. The dynamic response of the cable-stayed bridge is obtained by solving resulting nonlinear ordinary differential equations using Runge-Kutta-Felhberg method. Convergence of Galerkin method for VIV of the cable-stayed bridge is investigated. Numerical results show that there are significant influences of the stay cables on VIV of the deck beam: there are different limit cycles when one neglects geometric nonlinear terms associated with the stay cables, and there are only one limit cycle and chaotic responses in the case when the geometric nonlinear terms are considered.

2. Problem Formulation

Consider a cable-stayed bridge that consists of a simply supported four-cable-stayed deck beam and two towers, subjected to vortex shedding on the deck beam, as shown in Figure 1. The deck beam consists of seven segments separated by its junctions with the stay cables and towers. The following assumptions are made in this work in the formulation of the vibration problem of the cable-stayed bridge model subjected to vortex shedding:

(1) The cable-stayed bridge is modeled as a planar system.

(2) The towers, to which the stay cables are attached, are built on a hard rock foundation and can be assumed to be rigid [29, 30]; they are connected to the deck beam through roller supports.

(3) The stay cables and deck beam have linear elastic behaviors.

(4) Each segment of the deck beam obeys the Euler-Bernoulli beam theory.

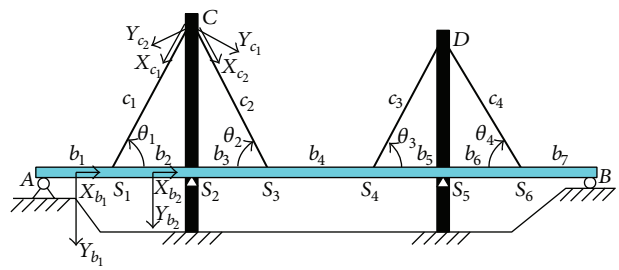

Figure 1: Schematic of a cable-stayed bridge that consists of a simply supported four-cable-stayed deck beam and two rigid towers.

2.1. Modeling of the Cable-Stayed Bridge. A free vibration analysis of the planar motion of this kind of cable-stayed bridges without considering vortex shedding was presented in [29]. The four stay cables are anchored to the deck beam at junctions S_1, S_3, S_4, and S_6, and the two towers are connected to the deck beam at junctions S_2 and S_5. The junctions $S_1, S_2, \ldots, S_6$ divide the deck beam into seven segments $b_1, b_2, \ldots, b_7$. The length, mass per unit length, elastic modulus, and cross-sectional area of the ith ($i = 1, 2, 3, 4$) stay cable are denoted by L_{c_i}, m_{c_i}, E_{c_i}, and A_{c_i}, respectively. The length, mass per unit length, elastic modulus, and area moment of inertia of the jth ($j = 1, 2, \ldots, 7$) segment of the deck beam are denoted by $2L_{b_j}$, m_{b_j}, E_{b_j}, and I_{b_j}, respectively.

Let (X_{c_i}, Y_{c_i}) be local coordinates of cable c_i in the vertical plane, with the origin located at point C for cables c_1 and c_2 and at point D for cables c_3 and c_4. Let (X_{b_j}, Y_{b_j}) be local coordinates of segment b_j of the deck beam in the vertical plane, with the origin located in the middle of segment b_j of the deck beam. Initial sags of the stay cables are considered. Under the assumption of a small ratio of sag D_{c_i} to length L_{c_i} (i.e., $D_{c_i}/L_{c_i} \leq 1/10$), the static equilibrium of the stay cable c_i can be approximated by a parabolic function $Y_{c_i}(X_{c_i}) = 4D_{c_i}[X_{c_i}/L_{c_i} - (X_{c_i}/L_{c_i})^2]$ in its domain, while the static deflection of the deck beam is assumed to be negligible. The dynamic configuration of the cable-stayed bridge model is completely described by longitudinal and transverse displacements of the stay cables $U_{c_i}(X_{c_i}, t)$ and $V_{c_i}(X_{c_i}, t)$, respectively, and transverse displacements of the segments of the deck beam $V_{b_j}(X_{b_j}, t)$, relative to the above equilibrium configuration.

The following nondimensional variables are introduced:

$$x_{c_i} = \frac{X_{c_i}}{L},$$

$$x_{b_j} = \frac{X_{b_j}}{L},$$

$$
\begin{aligned}
l_{c_i} &= \frac{L_{c_i}}{L}, \\
l_{b_j} &= \frac{L_{b_j}}{L}, \\
d_{c_i} &= \frac{D_{c_i}}{\Phi}, \\
y_{c_i} &= \frac{Y_{c_i}}{\Phi}, \\
u_{c_i} &= \frac{U_{c_i}}{\Phi}, \\
v_{c_i} &= \frac{V_{c_i}}{\Phi}, \\
v_{b_j} &= \frac{V_{b_j}}{\Phi}, \\
\tau &= \omega_0 t,
\end{aligned} \tag{1}
$$

where $L = \min\{L_{b_1}, L_{b_2}, \ldots, L_{b_7}\}$, $\omega_0 = (1/L_{b_1}^2)\sqrt{E_{b_1} I_{b_1}/m_{b_1}}$, and Φ is the diameter of stay cable c_1. Some additional nondimensional parameters need to be introduced to furnish a complete definition of elastodynamic properties of the cable-stayed bridge model:

$$
\begin{aligned}
\mu_{c_i} &= \frac{E_{c_i} A_{c_i}}{H_{c_i}}, \\
\chi_{c_i} &= \frac{7L^2 H_{c_i}}{\sum_{j=1}^{7} E_{b_j} I_{b_j}}, \\
\eta_{b_j} &= \frac{7E_{b_j} I_{b_j}}{\sum_{j=1}^{7} E_{b_j} I_{b_j}}, \\
\kappa &= \frac{\Phi}{L},
\end{aligned} \tag{2}
$$

where H_{c_i} is the tension in the stay cable c_i on which its initial sag is dependent; that is, $D_{c_i} = m_{c_i} g L_{c_i}^2 \cos\theta_i / 8H_{c_i}$, in which g is the acceleration of gravity. Since deck beam and cable materials of the cable-stayed bridge can generally be assumed to have different viscous damping behaviors, transverse damping coefficients of cable c_i and segment b_j of the deck beam are denoted by C_{c_i} and C_{b_j}, respectively, and their nondimensional parameters are defined by

$$
\begin{aligned}
\xi_{c_i} &= \frac{C_{c_i} \omega_0 L^2}{H_{c_i}}, \\
\xi_{b_j} &= \frac{C_{b_j} \omega_0 L^4}{E_{b_j} I_{b_j}},
\end{aligned} \tag{3}
$$

respectively.

The Newtonian method is used here to derive nonlinear equations of motion of the cable-stayed bridge model and a full set of geometric and dynamic boundary and matching conditions. Assuming that cable longitudinal inertial forces ($m_{c_i} \ddot{U}_{c_i}$) are negligible in the prevalent low-frequency transverse vibration of the cable-stayed bridge, the longitudinal cable displacement U_{c_i} can be statically condensed, leading to coupled nonlinear equations in terms of only the transversal cable and deck beam displacements V_{c_i} and V_{b_j}, respectively. The equations of motion of the cable-stayed bridge are [29]

$$
\beta_{c_i}^2 \ddot{v}_{c_i} + \xi_{c_i} \dot{v}_{c_i} - v_{c_i}'' - \mu_{c_i} e_{c_i}(\tau)\left(v_{c_i}'' + y_{c_i}''\right) = 0, \quad x_{c_i} \in \left[0, l_{c_i}\right], \tag{4}
$$

$$
\beta_{b_j}^4 \ddot{v}_{b_j} + \xi_{b_j} \dot{v}_{b_j} + v_{b_j}'''' = p_{b_j}\left(x_{b_j}, \tau, \dot{v}_{b_j}, \ddot{v}_{b_j}\right), \quad x_{b_j} \in \left[-l_{b_j}, l_{b_j}\right], \tag{5}
$$

where a prime and dot denote differentiation with respect to nondimensional local abscissae x_{c_i} and x_{b_j} and the time τ, respectively,

$$
\begin{aligned}
\beta_{c_i} &= L\omega_0 \left(\frac{m_{c_i}}{H_{c_i}}\right)^{1/2}, \\
\beta_{b_j} &= L\left(\frac{m_{b_j}\omega_0^2}{E_{b_j} I_{b_j}}\right)^{1/4}, \\
p_{b_j}&\left(x_{b_j}, \tau, \dot{v}_{b_j}, \ddot{v}_{b_j}\right) \\
&= \frac{L^4 P_{b_j}\left(X_{b_j}, t, dV_{b_j}/dt, d^2V_{b_j}/dt^2\right)}{E_{b_j} I_{b_j} \Phi}.
\end{aligned} \tag{6}
$$

The uniform cable elongation $e_{c_i}(\tau)$ in (4), which results from the static condensation procedure, instantaneously depends on both the beam tip deflection and the cable transverse displacement through the integral form [29]

$$
\begin{aligned}
e_{c_i}(\tau) = &\frac{\kappa v_{c_i}\left(l_{c_i}, \tau\right)}{l_{c_i}} \tan\theta_i \\
&+ \frac{\kappa^2}{l_{c_i}} \int_0^{l_{c_i}} \left(y_{c_i}' v_{c_i}' + \frac{1}{2} v_{c_i}'^2\right) dx_{c_i}.
\end{aligned} \tag{7}
$$

The functions v_{c_i} and v_{b_j} satisfy the following geometric boundary conditions:

$$
\begin{aligned}
A\colon\ v_{b_1}\left(-l_{b_1}, \tau\right) &= 0, \\
v_{b_1}''\left(-l_{b_1}, \tau\right) &= 0,
\end{aligned} \tag{8}
$$

$$B: v_{b_7}\left(l_{b_7},\tau\right)=0, \quad v''_{b_7}\left(l_{b_7},\tau\right)=0, \tag{9}$$

$$C: v_{c_1}(0,\tau)=0, \quad v_{c_2}(0,\tau)=0, \tag{10}$$

$$D: v_{c_3}(0,\tau)=0, \quad v_{c_4}(0,\tau)=0. \tag{11}$$

The matching conditions at the junctions S_k, where $k = 1,3,4,6$, which involve cables c_i, where $i = 1,2,3,4$, respectively, are

$$v_{b_k}\left(l_{b_k},\tau\right)=v_{b_{k+1}}\left(-l_{b_{k+1}},\tau\right), \tag{12}$$

$$v'_{b_k}\left(l_{b_k},\tau\right)=v'_{b_{k+1}}\left(-l_{b_{k+1}},\tau\right), \tag{13}$$

$$\eta_k v''_{b_k}\left(l_{b_k},\tau\right)=\eta_{k+1} v''_{b_{k+1}}\left(-l_{b_{k+1}},\tau\right), \tag{14}$$

$$\begin{aligned}\eta_{b_k} v'''_{b_k}\left(l_{b_k},\tau\right)-\eta_{b_{k+1}} v'''_{b_{k+1}}\left(-l_{b_{k+1}},\tau\right)&=\frac{\chi_{c_i}\mu_{c_i}}{\kappa}e_{c_i}(\tau)\\ &\cdot\sin\theta_i\\ &+\chi_{c_i}\left[v'_{c_i}\left(l_{c_i},\tau\right)+\mu_{c_i}e_{c_i}(\tau)\left(v'_{c_i}\left(l_{c_i},\tau\right)+y'_{c_i}\left(l_{c_i}\right)\right)\right]\\ &\cdot\cos\theta_i.\end{aligned} \tag{15}$$

The matching conditions at the junctions S_k $(k = 2,5)$ with the roller supports are

$$v_{b_k}\left(l_{b_k},\tau\right)=0, \tag{16}$$

$$v_{b_{k+1}}\left(-l_{b_{k+1}},\tau\right)=0, \tag{17}$$

$$v'_{b_k}\left(l_{b_k},\tau\right)=v'_{b_{k+1}}\left(-l_{b_{k+1}},\tau\right), \tag{18}$$

$$\eta_{b_k} v''_{b_k}\left(l_{b_k},\tau\right)=\eta_{b_{k+1}} v''_{b_{k+1}}\left(-l_{b_{k+1}},\tau\right). \tag{19}$$

Equations (4) and (5) with the boundary and matching conditions in (8)–(19) describe the nonlinear forced vibration of the cable-stayed bridge. The equations governing the small amplitude vibration of the cable-stayed bridge can be obtained by linearizing (8) through (19) in the neighborhood of the equilibrium configuration. An extensive analysis of the free vibration of the cable-stayed bridge is presented in [29].

2.2. Modeling of the Vortex Shedding Force. The distributed vortex shedding force on the deck beam can be modeled using Ehsan-Scanlan's model [28]:

$$\begin{aligned}P\left(X_{b_j},t,V_{b_j},\frac{dV_{b_j}}{dt}\right)&=\frac{1}{2}\rho U^2(2D)\\ &\cdot\left[Y_1(K)\left(1-\varepsilon\frac{V_{b_j}^2}{D^2}\right)\frac{1}{U}\frac{dV_{b_j}}{dt}\right.\\ &\left.+Y_2(K)\frac{V_{b_j}}{D}+\frac{1}{2}C_L(K)\sin(\omega t+\theta)\right],\end{aligned} \tag{20}$$

where ρ is the air density; U is the mean wind speed; $K = \omega D/U$ is the reduced frequency during VIV, in which ω is the frequency of the dynamic response of the cable-stayed bridge subjected to vortex shedding; θ is the phase angle of the harmonic force due to vortex shedding; and $Y_1(K)$, ε, $Y_2(K)$, and $C_L(K)$ are aeroelastic parameters that can be determined through wind-tunnel tests. The parameters $Y_1(K)$ and ε are related to linear and nonlinear components of the aerodynamic damping term, respectively. In particular, ε takes into account the fact that VIV is self-limiting. The parameter $Y_2(K)$ represents the aerodynamic stiffness term. The parameter $C_L(K)$ is related to the amplitude of the harmonic force due to vortex shedding. According to [27], the second and third terms on the right-hand side of (20) have a negligible contribution to the response of the cable-stayed bridge at lock-in. Hence, at lock-in, (20) can be reduced to the following form:

$$\begin{aligned}&P\left(X_{b_j},t,V_{b_j},\frac{dV_{b_j}}{dt}\right)\\ &\quad=\frac{1}{2}\rho U^2(2D)\left[Y_1(K)\left(1-\varepsilon\frac{V_{b_j}^2}{D^2}\right)\frac{1}{U}\frac{dV_{b_j}}{dt}\right].\end{aligned} \tag{21}$$

The nondimensional force $p_{b_j}(x_{b_j},\tau,v_{b_j},\dot{v}_{b_j})$ in (5) can be written as

$$p_{b_j}\left(x_{b_j},\tau,v_{b_j},\dot{v}_{b_j}\right)=\alpha_{b_j}Y_1\left(1-\varepsilon\lambda_{b_j}^2 v_{b_j}^2\right)\dot{v}_{b_j}, \tag{22}$$

where

$$\alpha_{b_j}\left(x_{b_j}\right)=\frac{\omega_0\rho UDL^4}{E_{b_j}I_{b_j}}, \quad \lambda_{b_j}=\frac{\Phi}{D_{b_j}}. \tag{23}$$

3. Solution Method

Galerkin method is used to analyze the vibration of the cable-stayed bridge. The dynamic response of stay cables and segments of the deck beam are expressed by

$$v_{c_i}\left(\tau, x_{c_i}\right) = \sum_{s=1}^{N} q_s(\tau)\,\phi_{c_i}^{(s)}\left(x_{c_i}\right), \tag{24}$$

$$v_{b_j}\left(\tau, x_{b_j}\right) = \sum_{s=1}^{N} q_s(\tau)\,\phi_{b_j}^{(s)}\left(x_{b_j}\right), \tag{25}$$

where $\phi_{c_i}^{(s)}$ and $\phi_{b_j}^{(s)}$ are corresponding components of the sth eigenfunction of the linearized cable-stayed bridge model [29], and $q_s(\tau)$ are generalized coordinates. Substituting (24) into (4) yields

$$\begin{aligned}
&\beta_{c_i}^2\left(\sum_{s=1}^{N}\ddot{q}_s\phi_{c_i}^{(s)}\right) + \xi_{c_i}\left(\sum_{s=1}^{N}\dot{q}_s\phi_{c_i}^{(s)}\right) - \left(\sum_{s=1}^{N}q_s\phi_{c_i}^{(s)\prime\prime}\right)\\
&\quad - \frac{\mu_{c_i}\kappa}{l_{c_i}}\left[\tan\theta_i\left(\sum_{s=1}^{N}q_s\phi_{c_i}^{(s)}\left(l_{c_i}\right)\right)\right.\\
&\quad + \kappa\int_0^{l_{c_i}} y_{c_i}'\left(\sum_{s=1}^{N}q_s\phi_{c_i}^{(s)\prime}\right)dx_{c_i}\\
&\quad \left. + \frac{\kappa}{2}\int_0^{l_{c_i}}\left(\sum_{s=1}^{N}q_s\phi_{c_i}^{(s)\prime}\right)^2 dx_{c_i}\right]\left[\left(\sum_{s=1}^{N}q_s\phi_{c_i}^{(s)\prime\prime}\right) + y_{c_i}''\right]\\
&\quad = 0.
\end{aligned} \tag{26}$$

Substituting (25) into (5) yields

$$\begin{aligned}
&\beta_{b_j}^4\left(\sum_{s=1}^{N}\ddot{q}_s\phi_{b_j}^{(s)}\right) + \xi_{b_j}\left(\sum_{s=1}^{N}\dot{q}_s\phi_{b_j}^{(s)}\right) + \left(\sum_{s=1}^{N}q_s\phi_{b_j}^{(s)\prime\prime\prime\prime}\right)\\
&\quad = \alpha_{b_j}Y_1\left(1 - \varepsilon\lambda_{b_j}^2\left(\sum_{s=1}^{N}q_s\phi_{b_j}^{(s)}\right)^2\right)\left(\sum_{s=1}^{N}\dot{q}_s\phi_{b_j}^{(s)}\right).
\end{aligned} \tag{27}$$

Multiplying (26) by $\chi_{c_i}\phi_{c_i}^{(r)}(x_{c_i})$ and integrating the resulting equation with respect to x_{c_i} from 0 to l_{c_i}, multiplying (27) by $\eta_{b_j}\phi_{b_j}^{(r)}(x_{b_j})$ and integrating the resulting equation with respect to x_{b_j} from $-l_{b_j}$ to l_{b_j}, adding all the resulting equations, and using the following orthogonality relations of eigenfunctions of the linearized cable-stayed bridge model [29]:

$$\begin{aligned}
&\sum_{i=1}^{4}\chi_{c_i}\beta_{c_i}^2\int_0^{l_{c_i}}\phi_{c_i}^{(r)}\left(x_{c_i}\right)\phi_{c_i}^{(s)}\left(x_{c_i}\right)dx_{c_i} + \sum_{j=1}^{7}\eta_{b_j}\beta_{b_j}^4\\
&\quad\cdot\int_{-l_{b_j}}^{l_{b_j}}\phi_{b_j}^{(r)}\left(x_{b_j}\right)\phi_{b_j}^{(s)}\left(x_{b_j}\right)dx_{b_j} = M_s\delta_{sr},\\
&-\sum_{i=1}^{4}\chi_{c_i}\left[\int_0^{l_{c_i}}\phi_{c_i}^{(r)}\left(x_{c_i}\right)\phi_{c_i}^{(s)\prime\prime}\left(x_{c_i}\right)dx_{c_i}\right.\\
&\quad\left. - 8\mu_{c_i}\widehat{e}_{c_i}^{(s)}\frac{d_{c_i}}{l_{c_i}^2}\int_0^{l_{c_i}}\phi_{c_i}^{(r)}\left(x_{c_i}\right)dx_{c_i}\right] + \sum_{j=1}^{7}\eta_{b_j}\\
&\quad\cdot\int_{-l_{b_j}}^{l_{b_j}}\phi_{b_j}^{(r)}\left(x_{b_j}\right)\phi_{b_j}^{(s)\prime\prime\prime\prime}\left(x_{b_j}\right)dx_{b_j} = \omega_s^2 M_s\delta_{sr}
\end{aligned} \tag{28}$$

in which $\widehat{e}_{c_i}^{(s)} = \kappa(\phi_{c_i}^{(s)}(l_{c_i})/l_{c_i})\tan\theta_i + \kappa^2(1/l_{c_i})\int_0^{l_{c_i}} y_{c_i}'\phi_{c_i}^{\prime(s)}dx_{c_i}$, ω_s is the sth natural frequency of the linearized cable-stayed bridge model, M_s are positive constants, and δ_{sr} is the Kronecker delta; one can obtain spatially discretized equations of the cable-stayed bridge:

$$\mathbf{M}\ddot{\mathbf{q}} + \left[\mathbf{C} + \mathbf{C}^{\text{Aero}}\right]\dot{\mathbf{q}} + \mathbf{K}\mathbf{q} + \mathbf{N}^{\text{Q}} + \mathbf{N}^{\text{C}} + \mathbf{N}^{\text{Hy}} = 0, \tag{29}$$

where entries of the matrices $\mathbf{M}$, $\mathbf{C}$, $\mathbf{C}^{\text{Aero}}$, $\mathbf{K}$, $\mathbf{N}^{\text{Q}}$, $\mathbf{N}^{\text{C}}$ and $\mathbf{N}^{\text{Hy}}$ are

$$\begin{aligned}
M_{rs} &= M_s\delta_{sr},\\
C_{rs} &= \sum_{i=1}^{4}\chi_{c_i}\xi_{c_i}\int_0^{l_{c_i}}\phi_{c_i}^{(s)}\phi_{c_i}^{(r)}dx_{c_i} + \sum_{j=1}^{7}\eta_{b_j}\xi_{b_j}\int_{-l_{b_j}}^{l_{b_j}}\phi_{b_j}^{(s)}\phi_{b_j}^{(r)}dx_{b_j},\\
C_{rs}^{\text{Aero}} &= -\sum_{j=1}^{7}\eta_{b_j}Y_1\int_{-l_{b_j}}^{l_{b_j}}\alpha_{b_j}\phi_{b_j}^{(s)}\phi_{b_j}^{(r)}dx_{b_j},\\
K_{rs} &= \omega_s^2 M_{rs},\\
N_r^{\text{Q}} &= \sum_{i=1}^{4}\sum_{m=1}^{N}\sum_{n=1}^{N}\chi_{c_i}\mu_{c_i}q_m q_n\left(4\frac{d_{c_i}\kappa^2}{l_{c_i}^3}\int_0^{l_{c_i}}\phi_{c_i}^{(m)\prime}\phi_{c_i}^{(n)\prime}dx_{c_i}\int_0^{l_{c_i}}\phi_{c_i}^{(r)}dx_{c_i} - \widehat{e}_{c_i}^{(m)}\int_0^{l_{c_i}}\phi_{c_i}^{(r)}\phi_{c_i}^{(n)\prime\prime}dx_{c_i}\right),\\
N_r^{\text{C}} &= -\kappa^2\sum_{i=1}^{4}\sum_{m=1}^{N}\sum_{n=1}^{N}\sum_{o=1}^{N}\frac{\chi_{c_i}\mu_{c_i}}{2l_{c_i}}q_m q_n q_o\int_0^{l_{c_i}}\phi_{c_i}^{(m)\prime}\phi_{c_i}^{(n)\prime}dx_{c_i}\int_0^{l_{c_i}}\phi_{c_i}^{(r)}\phi_{c_i}^{(o)\prime\prime}dx_{c_i},\\
N_r^{\text{Hy}} &= \sum_{j=1}^{7}\sum_{m=1}^{N}\sum_{n=1}^{N}\sum_{o=1}^{N}\eta_{b_j}Y_1\varepsilon\lambda_{b_j}^2 q_m q_n\dot{q}_o\int_{-l_{b_j}}^{l_{b_j}}\alpha_{b_j}\phi_{b_j}^{(m)}\phi_{b_j}^{(n)}\phi_{b_j}^{(o)}\phi_{b_j}^{(r)}dx_{b_j},
\end{aligned} \tag{30}$$

respectively.

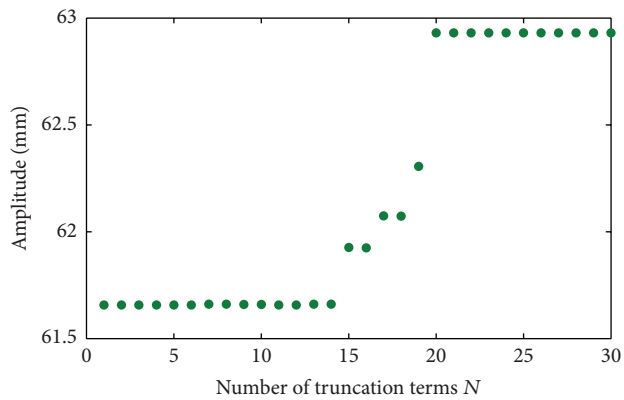

Figure 2: Effects of the number of Galerkin truncation terms on transverse displacements of the midpoint of the deck beam when there are no geometric nonlinear terms.

It should be noted that nonlinear terms $\mathbf{N}^{\mathrm{Q}}$ and $\mathbf{N}^{\mathrm{C}}$ in (29) are induced by geometric nonlinearities of the stay cables.

4. Numerical Simulation

Geometric and physical parameters of a cable-stayed bridge and aeroelastic parameters are listed in Table 1. It should be noted that a width-to-height ratio of 4 is used in this paper not only because it is a typical ratio of bridge decks but also because the cable-stayed bridge is supposed to have significant response amplitudes at lock-in [28]. For all the following calculation, modal damping ratio C_{rs} is always equal to $0.01\delta_{rs}$. The dynamic response of the cable-stayed bridge can be calculated from (29) using Runge-Kutta-Felhberg method in MATLAB, where initial conditions of generalized coordinates can be obtained from those of physical coordinates:

$$\begin{aligned} q_r(0) &= \frac{1}{M_r}\left[\sum_{i=1}^{4}\chi_{c_i}\beta_{c_i}^2\int_0^{l_{c_i}} v_{c_i}\left(x_{c_i},0\right)\phi_{c_i}^{(r)}\left(x_{c_i}\right)dx_{c_i}\right. \\ &\quad \left.+\sum_{j=1}^{7}\eta_{b_j}\beta_{b_j}^4\int_{-l_{b_j}}^{l_{b_j}} v_{b_j}\left(x_{b_j},0\right)\phi_{b_j}^{(r)}\left(x_{b_j}\right)dx_{b_j}\right], \\ \dot{q}_r(0) &= \frac{1}{M_r}\left[\sum_{i=1}^{4}\chi_{c_i}\beta_{c_i}^2\int_0^{l_{c_i}} \dot{v}_{c_i}\left(x_{c_i},0\right)\phi_{c_i}^{(r)}\left(x_{c_i}\right)dx_{c_i}\right. \\ &\quad \left.+\sum_{j=1}^{7}\eta_{b_j}\beta_{b_j}^4\int_{-l_{b_j}}^{l_{b_j}} \dot{v}_{b_j}\left(x_{b_j},0\right)\phi_{b_j}^{(r)}\left(x_{b_j}\right)dx_{b_j}\right]. \end{aligned} \tag{31}$$

For all the following calculation, $\dot{q}_r(0)$ is always equal to zero. Numerical simulations for two cases are undertaken: (1) neglecting the geometric nonlinear terms (i.e., $\mathbf{N}^{\mathrm{Q}} = \mathbf{N}^{\mathrm{C}} = \mathbf{0}$ in (29)) and (2) considering the geometric nonlinear terms.

4.1. Case Studies Neglecting the Geometric Nonlinear Terms. Convergence of Galerkin method for given initial conditions $q_r(0) = 0.1\delta_{r1}$, which means that the cable-stayed bridge has its initial dynamic configuration corresponding to its first mode shape and it is released from rest, is shown in Figures 2 and 3. The amplitudes of the steady-state transverse displacements of the midpoint of the deck beam with different numbers of Galerkin truncation terms, which are set to one through 30, are shown in Figure 2. As shown in Figure 2, the transverse displacements of the midpoint of the deck beam initially remain stable until the truncation number increases to 15 and suddenly increase to their converged values. A truncation with 20 terms can provide accurate results in analyzing the dynamic response of the deck beam. The difference between the amplitudes of two limit cycles obtained by truncation with one term and 20 terms is 1.94%, which is small. One can come to a conclusion that a truncation with one term is accurate enough for calculation of the steady-state response of the cable-stayed bridge when its initial dynamic configuration corresponds to its first mode shape. In other words, most of the energy of the cable-stayed bridge is concentrated in its first mode in this case. Phase portraits of the response of the midpoint of the deck beam for different numbers of Galerkin truncation terms, which is shown in Figure 3, also lead to the same conclusion. Other results that are not shown here for the sake of brevity indicate that Galerkin truncation with 20 terms yields accurate results for the dynamic response of the cable-stayed bridge in the following cases in this section. Hence, in the following numerical calculations in this section, the first 20 modes of the linearized undamped cable-stayed bridge model are used in Galerkin method. Time history responses of the midpoint of the deck beam when the initial dynamic configuration of the cable-stayed bridge corresponds to its first mode shape but has different amplitudes, that is, $q_1(0) = 0.1$ (the initial displacement of the midpoint of the deck beam is 32 mm) and $q_1(0) = 3$ (the initial displacement of the midpoint of the deck beam is 946 mm, which is rather large), are shown in Figures 4 and 5, respectively. It can be seen that the solutions with different $q_1(0)$ converge to the same limit cycle after long-time integration. The magnitudes of Floquet multipliers are all less than unity; the aforementioned limit cycle is asymptotically stable.

Solutions of a reduced-order model for a flow dynamic system can converge to a spurious limit cycle after long-time integration, even if it is initialized with a correct configuration

Table 1: Geometric and physical parameters of the cable-stayed bridge and aeroelastic parameters.

	Parameter	Unit	Value
Deck beam	Mass per unit length of the deck beam (m_{b_j})	kg/m	16940
	Elastic modulus of the deck beam (E_{b_j})	N/m^2	2.0×10^{11}
	Area moment of inertia of the deck beam (I_{b_j})	m^4	1.20
	Length of segment b_1 of the deck beam ($2L_{b_1}$)	m	35
	Length of segment b_2 of the deck beam ($2L_{b_2}$)	m	40
	Length of segment b_3 of the deck beam ($2L_{b_3}$)	m	50
	Length of segment b_4 of the deck beam ($2L_{b_4}$)	m	50
	Length of segment b_5 of the deck beam ($2L_{b_5}$)	m	50
	Length of segment b_6 of the deck beam ($2L_{b_6}$)	m	40
	Length of segment b_7 of the deck beam ($2L_{b_7}$)	m	35
Stay cables	Mass per unit length of the stay cables (m_{c_i})	kg/m	286
	Elastic modulus of the stay cables (E_{c_i})	N/m^2	2.0×10^{11}
	Cross-sectional area of the stay cables (A_{c_i})	m^2	0.0362
	Length of stay cable c_1 (L_{c_1})	m	52
	Length of stay cable c_2 (L_{c_2})	m	60
	Length of stay cable c_3 (L_{c_3})	m	60
	Length of stay cable c_4 (L_{c_4})	m	52
	Sag-to-span ratios of the stay cables ($\bar{d}_{c_i} = D_{c_i}/L_{c_i}$)		0.01
Aeroelastic parameters	Air density (ρ)	kg/m^3	1.205
	ε		1122.5 [28]
	Y_1		6.88 [28]

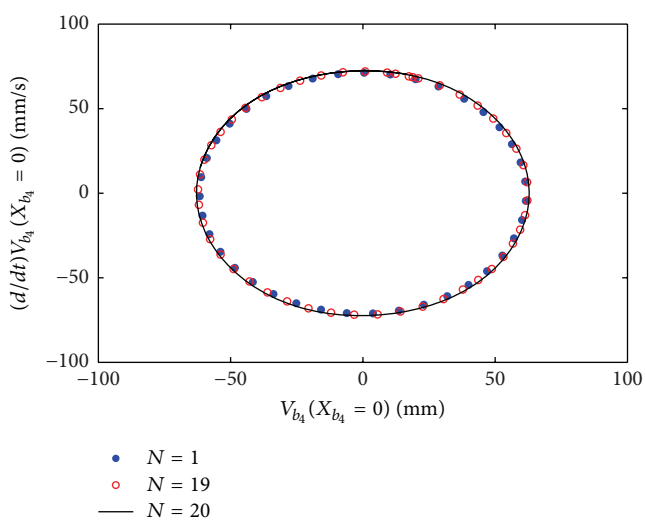

Figure 3: Phase portraits of the response of the midpoint of the deck beam for different numbers of Galerkin truncation terms, $q_r(0) = 0.1\delta_{1r}$.

[31, 32]. Sirisup and Karniadakis [32] demonstrated that the onset of divergence from the correct limit cycle depends on the number of Galerkin truncation terms, the Reynolds number, and the flow geometry. Since the limit cycle here does not vanish even when the truncation number is 30, which is large, one can conclude that the aforementioned limit cycle for the cable-stayed bridge is a correct one.

In many cases, higher mode shapes of the cable-stayed bridge would be excited; one such case is that when there are vehicles moving on the deck beam of the bridge. Hence, the initial dynamic configuration of the cable-stayed bridge can correspond to its higher mode shapes in the dynamic analysis of the cable-stayed bridge subjected to a distributed vortex shedding force. It is obvious that Galerkin truncation with one term is not enough in these cases. Through the same method with $N = 20$, one can find that there is the same limit cycle as that in Figure 3 when the initial dynamic configuration corresponds to the second through sixth mode shapes, and there is a different limit cycle when the initial dynamic configuration corresponds to the seventh

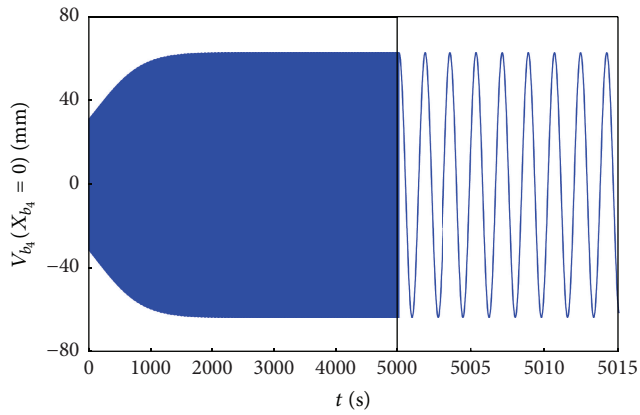

Figure 4: Time response of the midpoint of the deck beam, $q_r(0) = 0.1\delta_{1r}$.

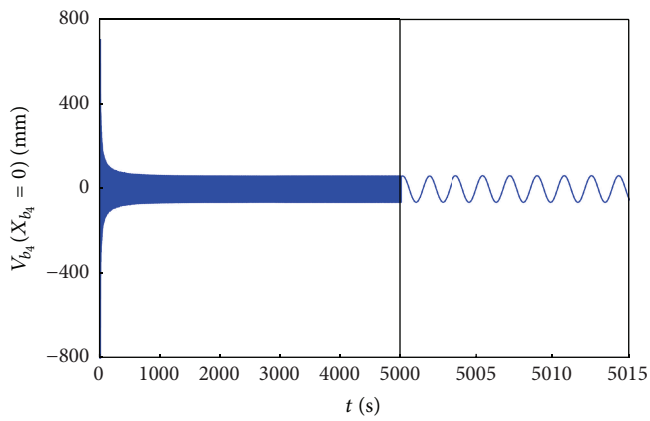

Figure 5: Time response of the midpoint of the deck beam, $q_r(0) = 3\delta_{1r}$.

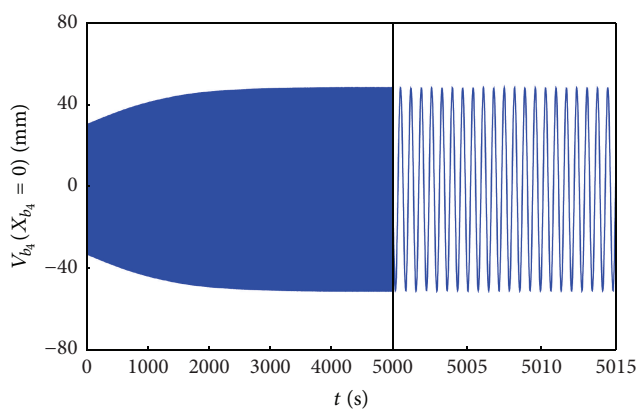

Figure 6: Time response of the midpoint of the deck beam, $q_r(0) = 0.1\delta_{7r}$.

mode shape (Figures 6 and 7). Two-dimensional projections of phase portraits onto the $(q_r, \dot{q}_r)$ plane when $q_r(0) = 0.1\delta_{1r}$ and $q_r(0) = 0.1\delta_{7r}$ are shown in Figures 8 and 9, respectively. Results when $q_r(0)$ is equal to $0.1\delta_{2r}$, $0.1\delta_{3r}, \ldots$, and $0.1\delta_{6r}$ are the same as that when $q_r(0) = 0.1\delta_{1r}$; they are not shown here for the sake of brevity. It can be seen from Figures 8 and 9 that energy of the cable-stayed bridge is concentrated in the first mode (the seventh mode) when its initial dynamic configuration corresponds to the first through sixth mode shapes (the seventh mode shape).

4.2. Case Studies Considering the Geometric Nonlinear Terms. Convergence of Galerkin method for given initial conditions $q_r(0) = 0.1\delta_{r1}$ is shown in Figures 10 and 11. The amplitudes of the steady-state transverse displacements of the midpoint of the deck beam with different numbers of Galerkin

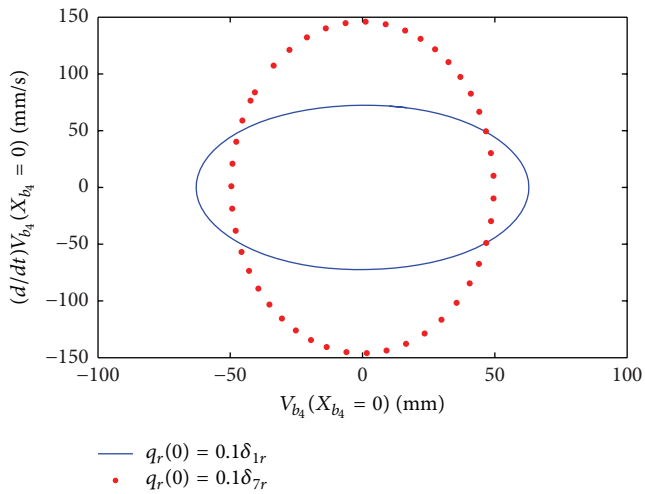

Figure 7: Two different stable limit cycles corresponding to different initial configurations.

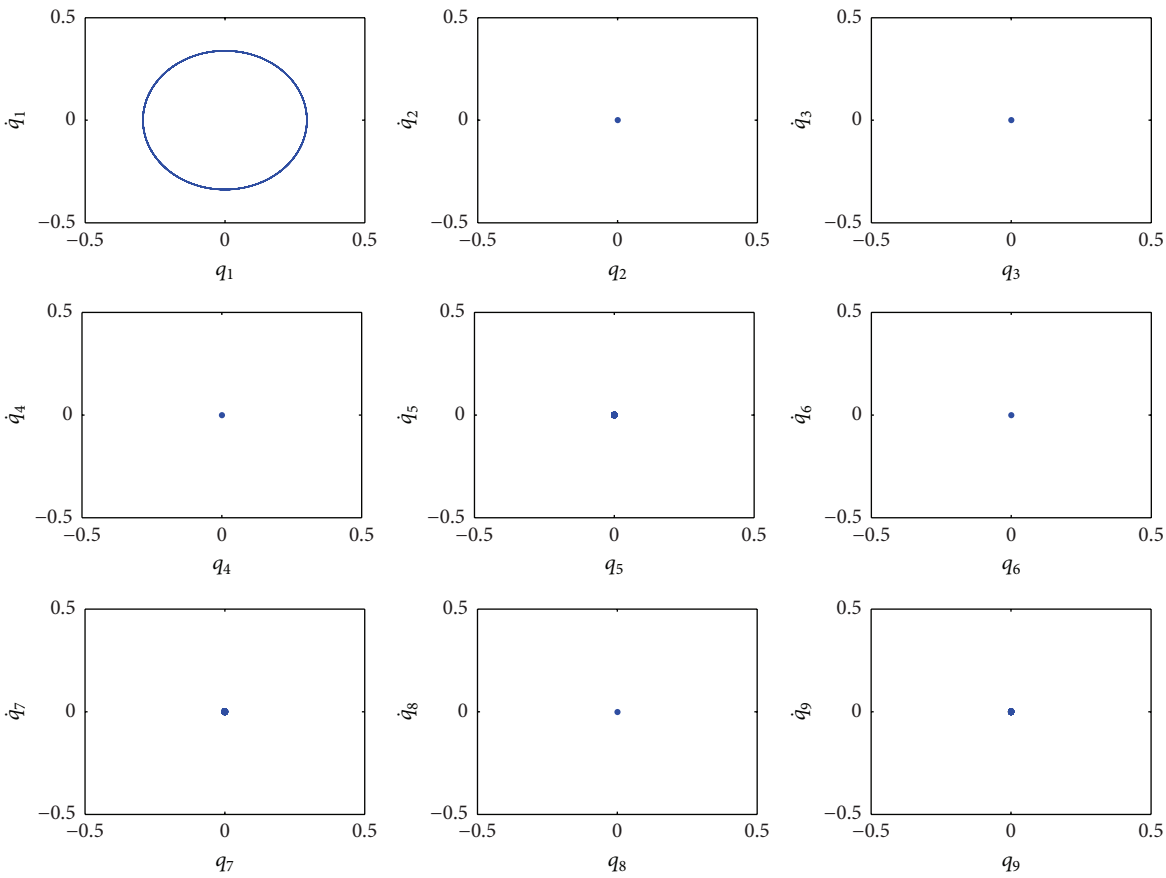

Figure 8: Two-dimensional projections of phase portraits onto the $(q_r, \dot{q}_r)$ plane, $q_r(0) = 0.1\delta_{1r}$.

truncation terms, which are set to one through 30, are shown in Figure 10. As shown in Figure 10, a truncation with 11 terms can provide accurate results in analyzing the dynamic response of the cable-stayed bridge, and it is much less than the cases in Section 4.1 where the geometric nonlinear terms are neglected. Phase portraits of the response of the midpoint of the deck beam for different numbers of Galerkin truncation terms, which are shown in Figure 11, also lead to the same conclusion. It can be noted from Figure 11 that the limit cycle becomes more asymmetric when the number of the truncation terms increases. The reason for this is that when the number of truncation terms increases to 7, an additional asymmetric limit cycle appears on the $(q_7, \dot{q}_7)$ plane which phase portraits project onto (see Figure 12 with

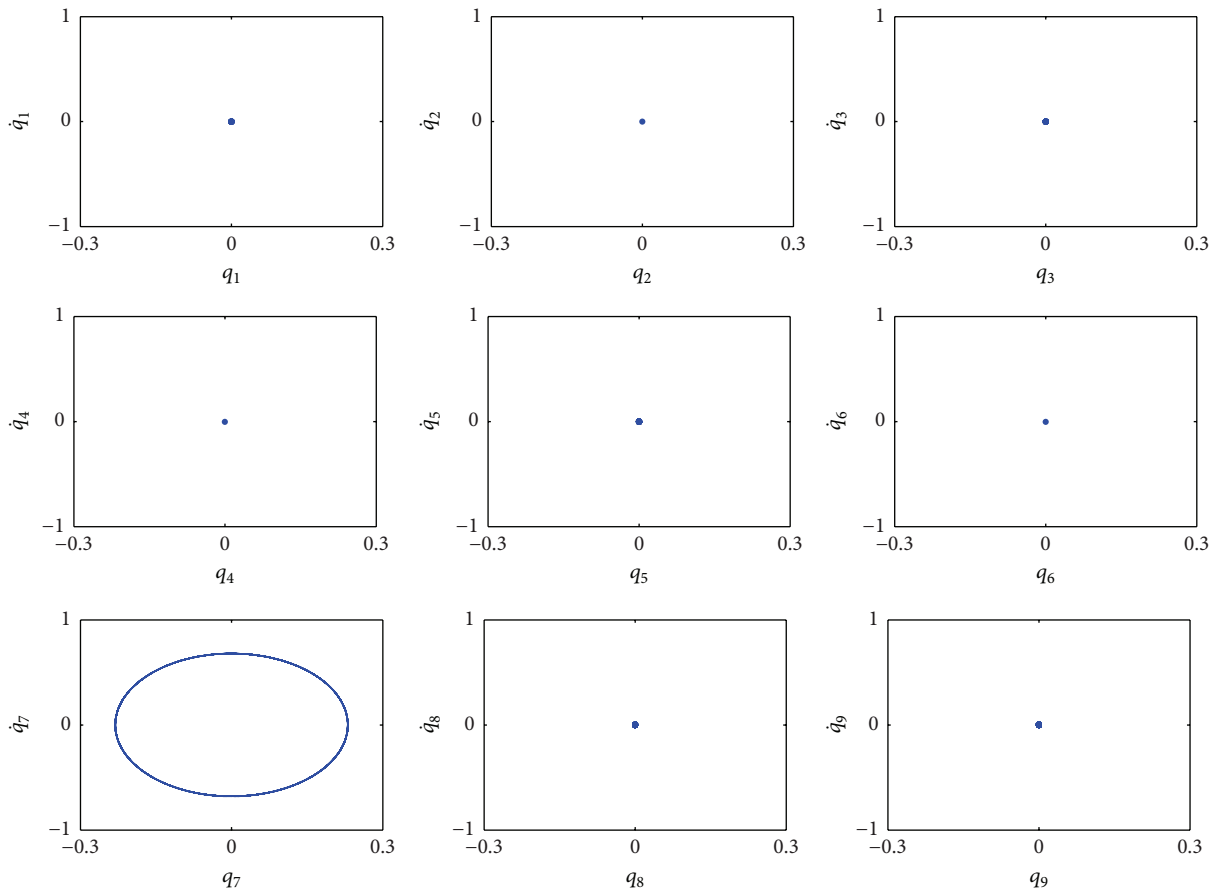

FIGURE 9: Two-dimensional projections of phase portraits onto the $(q_r, \dot{q}_r)$ plane, $q_r(0) = 0.1\delta_{7r}$.

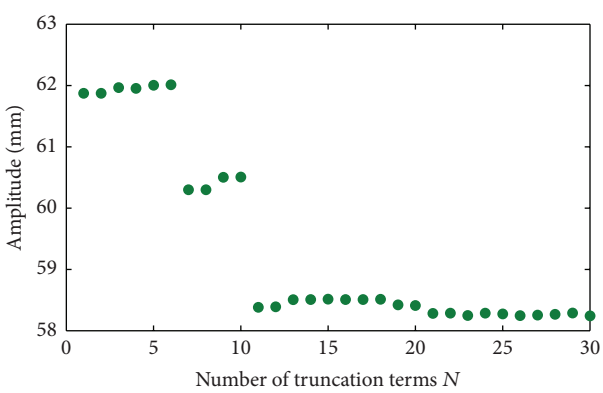

FIGURE 10: Effects of the number of Galerkin truncation terms on transverse displacements of the midpoint of the deck beam when there are geometric nonlinear terms.

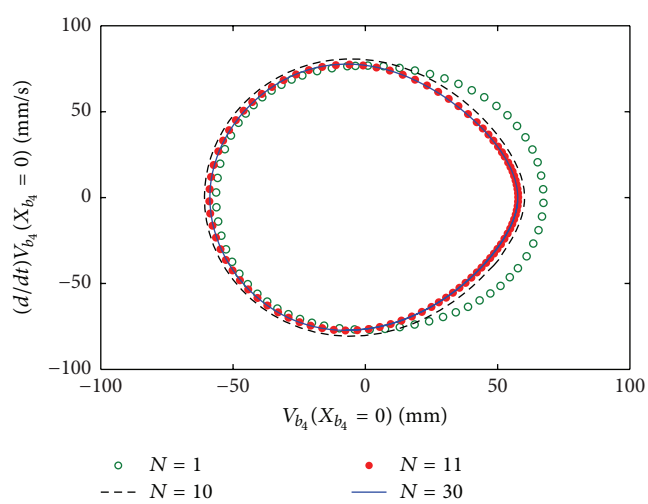

FIGURE 11: Phase portraits of the response of the midpoint of the deck beam for different numbers of Galerkin truncation terms, $q_r(0) = 0.1\delta_{1r}$.

$N = 11$). As shown in Figures 11 and 13, the dynamic response of the midpoint of the deck beam approaches a stable limit cycle. The bifurcation diagram of limit cycles with respect to $q_1(0)$ is shown in Figure 14 when the initial dynamic configuration of the cable-stayed bridge corresponds to its first mode shape. One can find from Figure 14 that when $q_1(0)$ is smaller than 0.27, a stable periodic solution exists, and when $q_1(0)$ is larger than or equal to 0.27, chaotic responses occur. For instance, when $q_1(0) = 0.3$ and $N = 11$, phase portraits of the response of the midpoint of the deck beam are shown in Figure 15, which indicates occurrence of chaotic

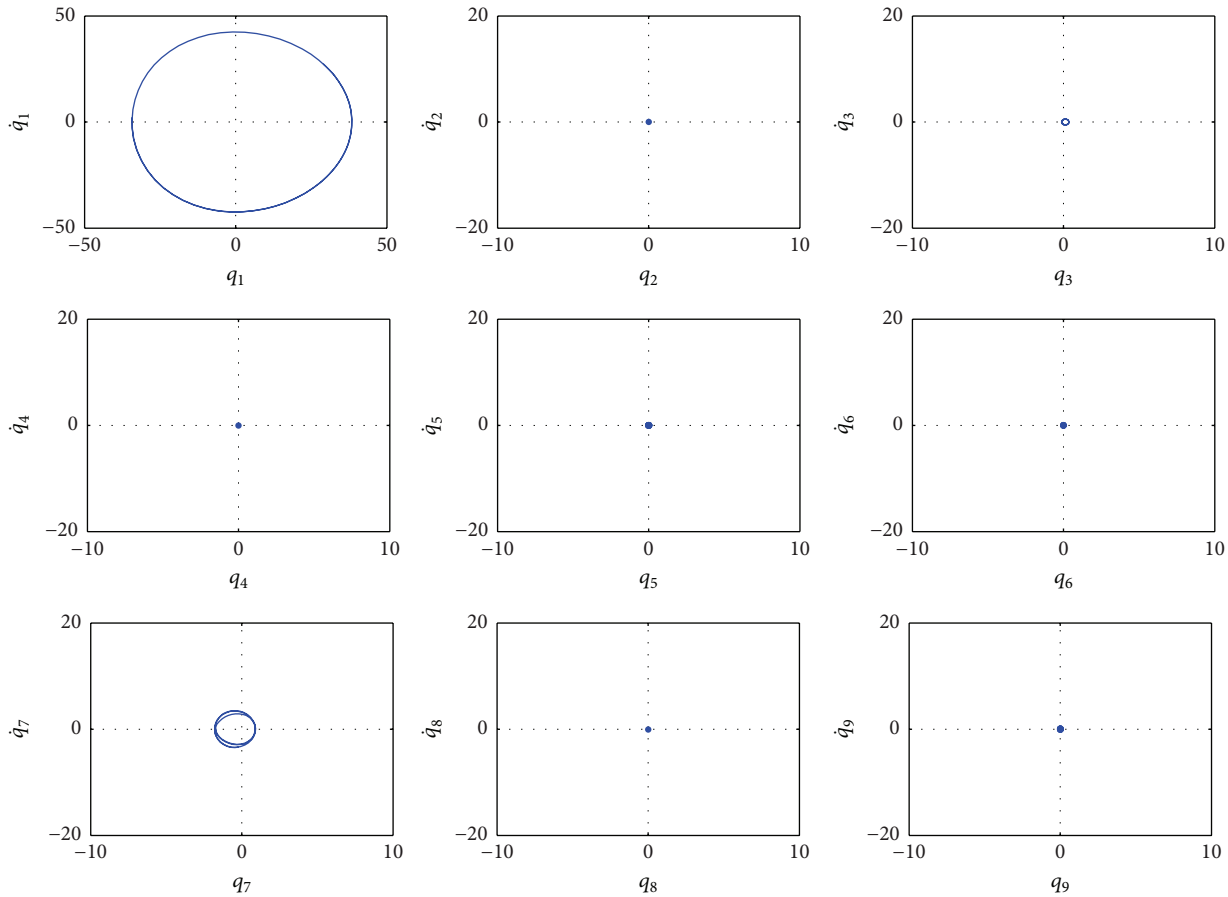

FIGURE 12: Two-dimensional projections of phase portraits onto the $(q_r, \dot{q}_r)$ plane, $q_r(0) = 0.1\delta_{1r}$ and $N = 11$.

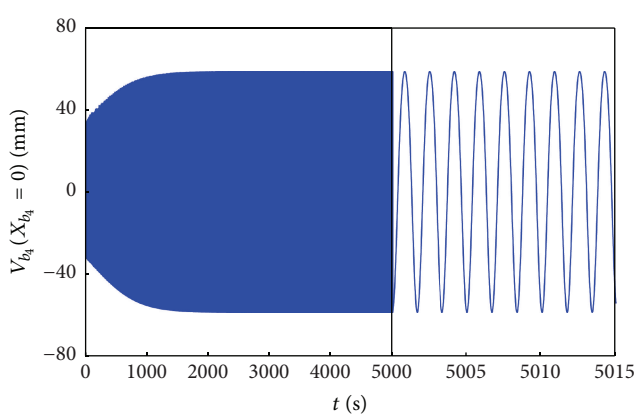

FIGURE 13: Time response of the midpoint of the deck beam; $q_r(0) = 0.1\delta_{1r}$ and $N = 11$.

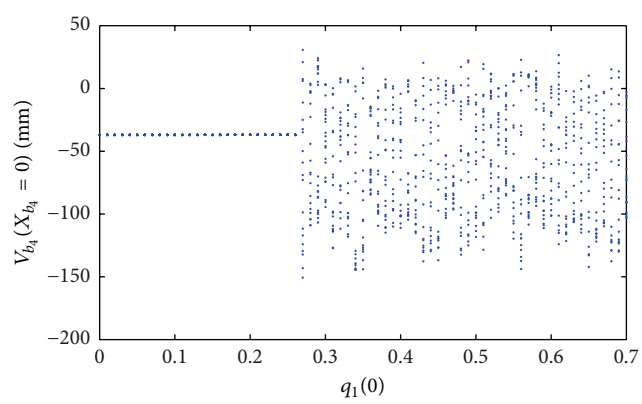

FIGURE 14: Bifurcation diagram of the cable-stayed bridge with respect to $q_1(0)$, $q_r(0) = q_1(0)\delta_{1r}$ and $N = 11$.

response. On the contrary, for a truncation with one term, the response always approaches a stable limit cycle no matter how large the amplitude of the initial dynamic configuration is (see Figures 16–18). These mean that the true dynamic response of the cable-stayed bridge may not be captured by the truncation with one term even when the initial dynamic configuration corresponds to the first mode shape. When the initial dynamic configuration of the cable-stayed bridge corresponds to one of its higher mode shapes, chaotic response occurs even if its amplitude is relatively small; this is shown in Figure 19 where the initial dynamic configuration of the cable-stayed bridge corresponds to its second mode shape and its magnitude is only 0.1.

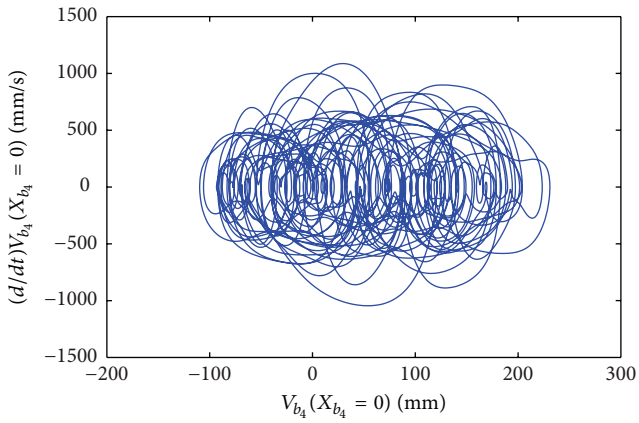

Figure 15: Chaotic response of the midpoint of the deck beam, $q_r(0) = 0.3\delta_{1r}$.

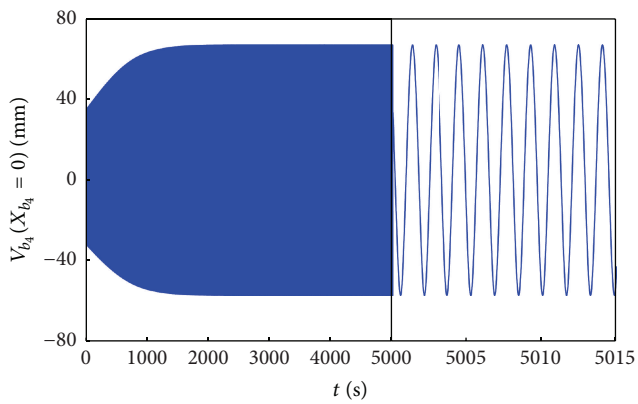

Figure 16: Time response of the midpoint of the deck beam, $q_1(0) = 0.1$ and $N = 1$.

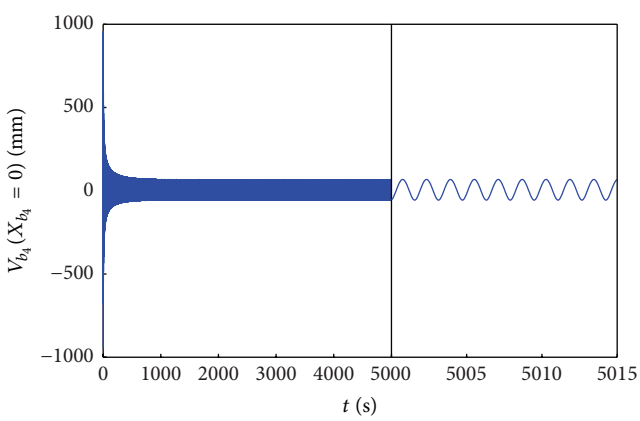

Figure 17: Time response of the midpoint of the deck beam, $q_1(0) = 3$ and $N = 1$.

5. Conclusions

The dynamic behavior of a cable-stayed bridge that consists of a simply supported four-cable-stayed deck beam and two rigid towers subjected to a distributed vortex shedding force on the deck beam has been investigated. The

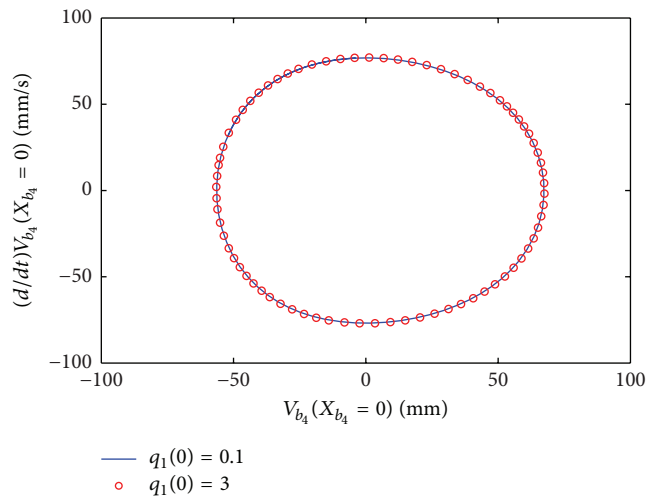

Figure 18: Phase portraits of the response of the midpoint of the deck beam for different initial conditions, $N = 1$.

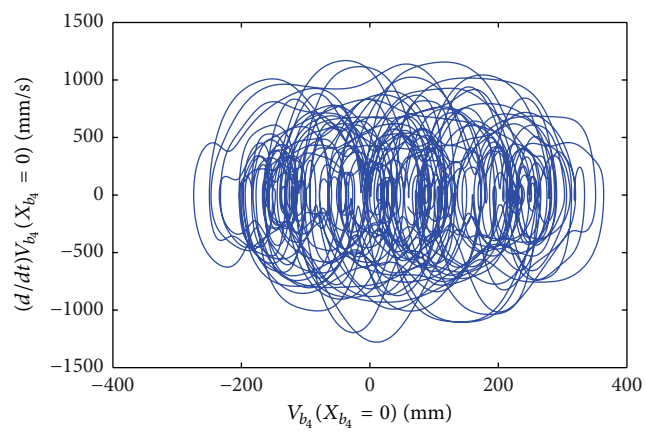

Figure 19: Chaotic response of the midpoint of the deck beam, $q_r(0) = 0.1\delta_{2r}$.

dynamic response of the cable-stayed bridge is calculated using Galerkin method in conjunction with Runge-Kutta-Felhberg method in MATLAB. Convergence of Galerkin method for the dynamic response of the cable-stayed bridge is studied. Numerical simulations show that the geometric nonlinearities of the stay cables have significant influence on VIV of the cable-stayed bridge, and further conclusions can be summarized as follows:

(1) In the case when the geometric nonlinear terms are neglected, accurate calculation of the response amplitude of the cable-stayed bridge at lock-in only needs use of the first mode shape of the linearized undamped cable-stayed bridge model when the initial dynamic configuration of the cable-stayed bridge corresponds to its mode shape whose mode number is smaller than seven. There is a different limit cycle when the initial dynamic configuration corresponds to its mode shape whose mode number is equal to or larger than 7.

(2) In the case when the geometric nonlinear terms are considered, calculation of the response of the cable-stayed bridge generally needs use of multiple mode shapes of the linearized undamped cable-stayed bridge model even when the initial dynamic configuration of the cable-stayed bridge corresponds to its first mode shape. There is a limit cycle when the initial dynamic configuration of the cable-stayed bridge corresponds to its first mode shape and its amplitude is smaller than 0.3 for the generalized coordinate, and there is chaotic response when the initial dynamic configuration of the cable-stayed bridge corresponds to its first mode shape with its amplitude larger than 0.3 for the generalized coordinate or one of its higher mode shapes.

Conflict of Interests

The authors declare that there is no conflict of interests regarding publication of this paper.

Acknowledgments

This work is supported by the National Natural Science Foundation of China under Grant nos. 11302087 and 11442006, the Natural Science Foundation of Jiangsu Province under Grant no. BK20130479, the Research Foundation for Advanced Talents of Jiangsu University under Grant no. 13JDG068, and the National Science Foundation under Grant no. CMMI-1000830.

References

[1] K. Y. R. Billah and R. H. Scanlan, "Resonance, Tacoma Narrows Bridge failure, and undergraduate physics textbooks," *American Journal of Physics*, vol. 59, no. 2, pp. 118–124, 1991.

[2] R. D. Blevins, *Flow-Induced Vibration*, Krieger, New York, NY, USA, 2nd edition, 1994.

[3] H. Zheng, R. E. Price, Y. Modarres-Sadeghi, and M. S. Triantafyllou, "On fatigue damage of long flexible cylinders due to the higher harmonic force components and chaotic vortex-induced vibrations," *Ocean Engineering*, vol. 88, pp. 318–329, 2014.

[4] C. Evangelinos, D. Lucor, and G. E. Karniadakis, "DNS-derived force distribution on flexible cylinders subject to vortex-induced vibration," *Journal of Fluids and Structures*, vol. 14, no. 3, pp. 429–440, 2000.

[5] H. M. Blackburn, R. N. Govardhan, and C. H. K. Williamson, "A complementary numerical and physical investigation of vortex-induced," *Journal of Fluids and Structures*, vol. 15, no. 3-4, pp. 481–488, 2001.

[6] R. H. J. Willden and J. M. R. Graham, "Numerical prediction of VIV on long flexible circular cylinders," *Journal of Fluids and Structures*, vol. 15, no. 3-4, pp. 659–669, 2001.

[7] E. Guilmineau and P. Queutey, "A numerical simulation of vortex shedding from an oscillating circular cylinder," *Journal of Fluids and Structures*, vol. 16, no. 6, pp. 773–794, 2002.

[8] I. Jadic, R. M. C. So, and M. P. Mignolet, "Analysis of fluid—structure interactions using a time-marching technique," *Journal of Fluids and Structures*, vol. 12, no. 6, pp. 631–654, 1998.

[9] C. Y. Zhou, R. M. C. So, and K. Lam, "Vortex-induced vibrations of an elastic circular cylinder," *Journal of Fluids and Structures*, vol. 13, no. 2, pp. 165–189, 1999.

[10] J. R. Meneghini and P. W. Bearman, "Numerical simulation of high amplitude oscillatory flow about a circular cylinder," *Journal of Fluids and Structures*, vol. 9, no. 4, pp. 435–455, 1995.

[11] T. Sarpkaya, "Computational methods with vortices," *Journal of Fluids Engineering*, vol. 111, no. 1, pp. 5–52, 1989.

[12] T. Sarpkaya, "Vortex element methods for flow simulation," *Advances in Applied Mechanics*, vol. 31, pp. 113–247, 1994.

[13] R. D. Gabbai and H. Benaroya, "An overview of modeling and experiments of vortex-induced vibration of circular cylinders," *Journal of Sound and Vibration*, vol. 282, no. 3–5, pp. 575–616, 2005.

[14] R. H. Scanlan, "On the state-of-the-art methods for calculations of flutter, vortex-induced and buffeting response of bridge structures," Tech. Rep. FHWA/RD-80/050, National Technical Information Service, Springfield, Va, USA, 1981.

[15] R. H. Scanlan, "Bridge flutter derivatives at vortex lock-in," *Journal of Structural Engineering*, vol. 124, no. 4, pp. 450–458, 1998.

[16] B. J. Vickery and R. I. Basu, "Across-wind vibrations of structures of circular cross-section. Part I. Development of a mathematical model for two-dimensional conditions," *Journal of Wind Engineering and Industrial Aerodynamics*, vol. 12, no. 1, pp. 49–73, 1983.

[17] A. Larsen, "A generalized model for assessment of vortex-induced vibrations of flexible structures," *Journal of Wind Engineering and Industrial Aerodynamics*, vol. 57, no. 2-3, pp. 281–294, 1995.

[18] T. Sarpkaya, "Fluid forces on oscillating cylinders," *Journal of Waterway, Port, Coastal, and Ocean Division (ASCE)*, vol. 104, no. 3, pp. 275–290, 1978.

[19] T. Staubli, "Calculation of vibration of an elastically mounted cylinder using experimental data from a forced oscillation," *Journal of Fluids Engineering*, vol. 105, no. 2, pp. 225–229, 1983.

[20] W. D. Iwan and D. L. R. Botelho, "Vortex-induced oscillation of structures in water," *Journal of Waterway, Port, Coastal and Ocean Engineering*, vol. 111, no. 2, pp. 289–303, 1985.

[21] R. T. Hartlen and I. G. Currie, "Lift-oscillator model of vortex-induced vibration," *Journal of Engineering Mechanics Division (ASCE)*, vol. 96, no. 5, pp. 577–591, 1970.

[22] R. A. Skop and O. M. Griffin, "A model for the vortex-excited resonant response of bluff cylinders," *Journal of Sound and Vibration*, vol. 27, no. 2, pp. 225–233, 1973.

[23] W. D. Iwan and R. D. Blevins, "A model for vortex induced oscillation of structures," *Journal of Applied Mechanics, Transactions ASME*, vol. 41, no. 3, pp. 581–586, 1974.

[24] E. H. Dowell, "Non-linear oscillator models in bluff body aeroelasticity," *Journal of Sound and Vibration*, vol. 75, no. 2, pp. 251–264, 1981.

[25] R. H. M. Ogink and A. V. Metrikine, "A wake oscillator with frequency dependent coupling for the modeling of vortex-induced vibration," *Journal of Sound and Vibration*, vol. 329, no. 26, pp. 5452–5473, 2010.

[26] X. Bai and W. Qin, "Using vortex strength wake oscillator in modelling of vortex induced vibrations in two degrees of freedom," *European Journal of Mechanics B/Fluids*, vol. 48, pp. 165–173, 2014.

[27] F. Ehsan and R. H. Scanlan, "Vortex–induced vibrations of flexible bridges," *Journal of Engineering Mechanics*, vol. 116, no. 6, pp. 1392–1411, 1990.

[28] A. M. Marra, C. Mannini, and G. Bartoli, "Van der Pol-type equation for modeling vortex-induced oscillations of bridge decks," *Journal of Wind Engineering and Industrial Aerodynamics*, vol. 99, no. 6-7, pp. 776–785, 2011.

[29] D. Q. Cao, M. T. Song, W. D. Zhu, R. W. Tucker, and C. H.-T. Wang, "Modeling and analysis of the in-plane vibration of a complex cable-stayed bridge," *Journal of Sound and Vibration*, vol. 331, no. 26, pp. 5685–5714, 2012.

[30] E. Caetano, A. Cunha, V. Gattulli, and M. Lepidi, "Cable-deck dynamic interactions at the International Guadiana Bridge: on-site measurements and finite element modelling," *Structural Control and Health Monitoring*, vol. 15, no. 3, pp. 237–264, 2008.

[31] I. Akhtar, A. H. Nayfeh, and C. J. Ribbens, "On the stability and extension of reduced-order Galerkin models in incompressible flows," *Theoretical and Computational Fluid Dynamics*, vol. 23, no. 3, pp. 213–237, 2009.

[32] S. Sirisup and G. E. Karniadakis, "A spectral viscosity method for correcting the long-term behavior of POD models," *Journal of Computational Physics*, vol. 194, no. 1, pp. 92–116, 2004.